

SUZAKU OBSERVATION OF THE NEW SOFT GAMMA REPEATER SGR 0501+4516 IN OUTBURST

T. ENOTO¹, Y.E. NAKAGAWA², N. REA³, P. ESPOSITO^{4,5}, D. GÖTZ⁶, K. HURLEY⁷, G.L. ISRAEL⁸, M. KOKUBUN⁹,
K. MAKISHIMA^{1,2}, S. MEREGHETTI⁴, H. MURAKAMI¹⁰, K. NAKAZAWA¹, T. SAKAMOTO¹¹, L. STELLA⁸,
A. TIENGO⁴, R. TUROLLA^{12,13}, S. YAMADA¹, K. YAMAOKA¹⁴, A. YOSHIDA¹⁴, AND S. ZANE¹³

Draft version October 18, 2018

ABSTRACT

We present the first *Suzaku* observation of the new Soft Gamma Repeater SGR 0501+4516, performed on 2008 August 26, four days after the onset of bursting activity of this new member of the magnetar family. The soft X-ray persistent emission was detected with the X-ray Imaging Spectrometer (XIS) at a 0.5–10 keV flux of 3.8×10^{-11} erg s⁻¹cm⁻², with a spectrum well fitted by an absorbed blackbody plus power-law model. The source pulsation was confirmed at a period of 5.762072 ± 0.000002 s, and 32 X-ray bursts were detected by the XIS, four of which were also detected at higher energies by the Hard X-ray Detector (HXD). The strongest burst, which occurred at 03:16:16.9 (UTC), was so bright that it caused instrumental saturation, but its precursor phase, lasting for about 200 ms, was detected successfully over the 0.5–200 keV range, with a fluence of $\sim 2.1 \times 10^{-7}$ erg cm⁻² and a peak intensity of about 89 Crab. The entire burst fluence is estimated to be ~ 50 times higher. The precursor spectrum was very hard, and well modeled by a combination of two blackbodies. We discuss the bursting activity and X/ γ -ray properties of this newly discovered Soft Gamma Repeater in comparison with other members of the class.

Subject headings: pulsar: individual (SGR 0501+4516) — stars: magnetic fields — X-rays: stars

1. INTRODUCTION

A new Soft Gamma Repeater (SGR), SGR 0501+4516, was discovered on 2008 August 22 by the *Swift* Burst Alert Telescope, thanks to the detection of many short bursts (Holland and Sato 2008; Barthelmy et al. 2008). Archival *ROSAT* data showed a faint X-ray source consistent with the position of this new SGR, probably its quiescent counterpart (Kennea & Mangano 2008).

SGRs are a sub-class of the so called “magnetars”, believed to be isolated neutron stars with very strong magnetic fields (10^{14-15} G; Thompson & Duncan 1995). This extreme magnetic field powers their bright emission, rather than accretion or rotational power as for most of

the X-ray pulsars. Only four confirmed SGRs are known to date, all sharing common properties with the other magnetars (the Anomalous X-ray Pulsars, aka AXPs) such as i) a spin period in a very small range of values (2–12 s), ii) large period derivatives ($10^{-13} - 10^{-11}$ s s⁻¹), iii) bright persistent X-ray emission (10^{33-36} erg s⁻¹), compared to the rather dim infrared counterparts, iv) unpredictable bursting and flaring activity, with a large range of energetics (10^{37-46} erg s⁻¹) and timescales (ms to years), and v) transient radio emission (sometimes pulsed) connected with their X-ray activity (Woods & Thompson 2006; Mereghetti 2008).

We report in this *Letter* on a *Suzaku* Target of Opportunity (ToO) observation of SGR 0501+4516, the first new SGR discovered in our Galaxy in the last ten years, which was performed only four days after the bursting activation.

2. OBSERVATION

A ToO observation of SGR 0501+4516 was performed with *Suzaku* (Mitsuda et al. 2007), on 2008 August 26 starting at 00:05 (UT), until August 27 08:25 (UT). The X-ray Imaging Spectrometer (XIS; Koyama et al. 2007) was operated in the normal mode with 1/4 window option, to ensure a time resolution of 2 s. The Hard X-ray Detector (HXD; Takahashi et al. 2007) was in the standard mode, wherein individual events have a time resolution of 61 μ s, and the four-channel HXD-WAM counts are available every 1 s. The target was placed at the “XIS nominal” position.

The XIS and HXD data were both processed with the *Suzaku* pipeline processing ver. 2.2.8.20. Events were discarded if they were acquired in the South Atlantic Anomaly, or in regions of low cutoff rigidity (≤ 6 GV for XIS and ≤ 8 GV for HXD), or with low Earth elevation angles. The net exposures obtained with the XIS and the HXD were 43 ks and 55 ks, respectively.

arXiv:0901.3453v1 [astro-ph.HE] 22 Jan 2009

¹ Department of Physics, University of Tokyo, 7-3-1 Hongo, Bunkyo-ku, Tokyo, 113-0033, Japan

² Cosmic Radiation Laboratory, Institute of Physical and Chemical Research (RIKEN), Wako, Saitama, 351-0198, Japan

³ Astronomical Institute “Anton Pannekoek”, University of Amsterdam, Kruislaan 403, 1098 SJ Amsterdam, The Netherlands

⁴ INAF–Istituto di Astrofisica Spaziale e Fisica Cosmica - Milano, via E. Bassini 15, 20133 Milano, Italy

⁵ INFN-Istituto Nazionale di Fisica Nucleare, Sezione di Pavia, via A. Bassi 6, 27100 Pavia, Italy

⁶ CEA Saclay, DSM/Irfu/Service d’Astrophysique, Orme des Merisiers, Bat. 709, 91191 Gif sur Yvette, France

⁷ Space Sciences Laboratory, 7 Gauss Way, University of California, Berkeley, CA 94720-7450, U.S.A.

⁸ INAF–Astronomical Observatory of Rome, via Frascati 33, 00040, Monteporzio Catone (RM), Italy

⁹ Institute of Space and Astronautical Science, JAXA, 3-1-1 Yoshinodai, Sagami-hara, Kanagawa, Japan 229-8510

¹⁰ Department of Physics, Rikkyo University, 3-34-1 Nishi-Ikebukuro, Toshima-ku, Tokyo, 171-8501, Japan

¹¹ NASA Goddard Space Flight Center, Greenbelt, MD 20771, U.S.A.

¹² University of Padua, Department of Physics, via Marzolo 8, 35131 Padua, Italy

¹³ MSSL, University College London, Holmbury St. Mary, Dorking Surrey, RH5 6NT, UK

¹⁴ Department of Physics & Mathematics, Aoyama Gakuin University, Sagami-hara, Kanagawa, 229-8558, Japan

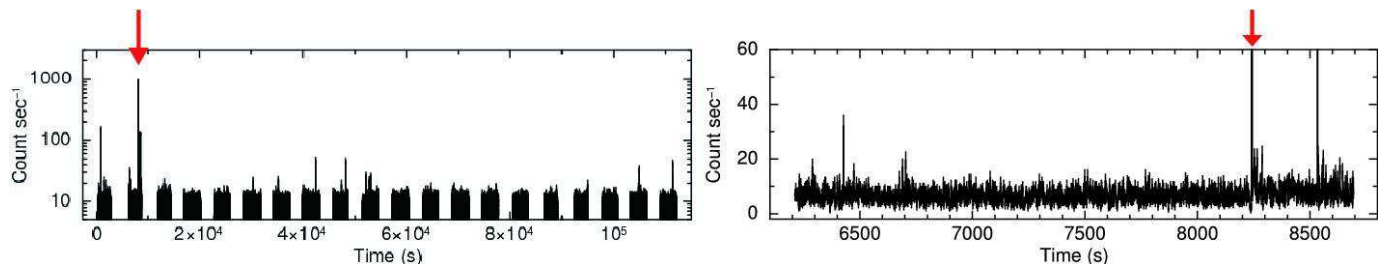


FIG. 1.— *Left*: 2-s binned 0.4–10 keV light-curve of the entire observation, obtained by summing events from all three XIS cameras. The largest burst is indicated by a red arrow. *Right*: A zoom of the ~ 3 ks of the left panel around the burst.

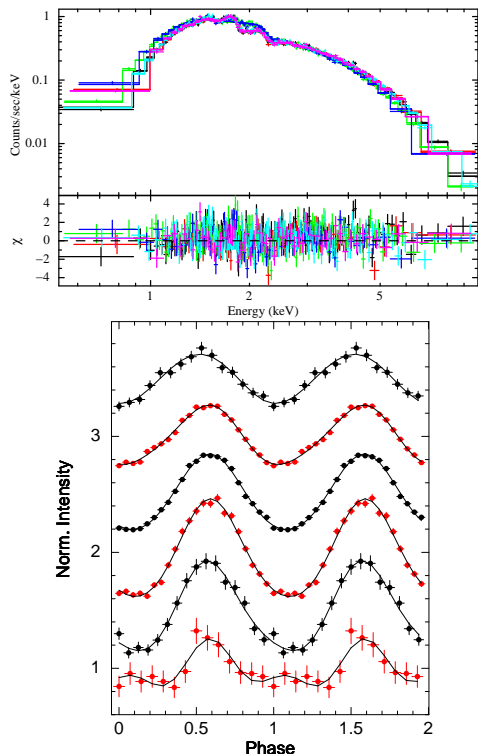


FIG. 2.— XIS results on the persistent emission from SGR 0501+4516. *Top panel*: All XIS spectra of the persistent emission (see text for details), simultaneously modeled with an absorbed blackbody plus power law. *Bottom panel*: Pulse profiles as a function of the energy band (from top to bottom: 0.5–1, 1–2, 2–3, 3–5, 5–8, and 8–12 keV).

3. ANALYSIS AND RESULTS

3.1. The persistent soft X-ray emission

The on-source XIS events were extracted from each of the 3 XIS cameras, over a region $1'.8$ in radius centered on the target position. The background events were derived from a similar region as far away from the source as possible.

We detected SGR 0501+4516 at a 0.4–10 keV count rate of $1.74 \text{ count s}^{-1}$ with each XIS front-illuminated (FI) CCD (XIS 0 and XIS 3), and $1.82 \text{ count s}^{-1}$ with the back-illuminated (BI) one (XIS 1). The 0.4–10 keV XIS light curve presented in Figure 1 reveals 32 short (≤ 2 s) burst episodes, where the count rate per 2 s, summed over the 3 cameras, increased by more than 5σ above the persistent emission (plus background). Several of them were also detected with the HXD (§3.2).

After eliminating the 32 bursts, we began the timing analysis (using *Xronos* 5.21) by converting all the event

arrival times to the Solar System barycenter. A power spectrum analysis confirmed the reported 5.76 s periodicity (Gögüş et al. 2008) in several harmonics. By folding the data at the fundamental period and employing a phase-fitting technique (Dall’Osso et al. 2003), the best-fit period was found to be $P = 5.762072 \pm 0.000002$ s at the 14704.0 TJD epoch (all uncertainties are at the 90% confidence level). This is consistent with those measured with *RXTE*, *Swift*, and *XMM-Newton* (Gögüş et al. 2008; Israel et al. 2008a).

Given the XIS timing resolution of 2 s, we cannot study detailed pulse profile sub-structures. However, looking at the 0.5–12 keV XIS profiles as a function of energy (Figure 2 bottom), we found that below about 5 keV one sinusoidal function at the fundamental spin frequency fit the profile shape well, while at higher energies the second harmonic component is needed at a significance of 4σ to reproduce the profile. The pulsed fraction (defined as the semi-amplitude of the fundamental sinusoidal modulation divided by the mean background-subtracted count rate) was 30(1)% on average, while it varied with energy as 21(3), 24(2), 30(2), 43(1), 30(3), and 20(3)%, at 0.4–1, 1–2, 2–3, 3–5, 5–7, and 7–10 keV, respectively.

Soft X-ray spectra of the persistent emission were studied with *XSPEC12*. We modeled the background-subtracted XIS-FI (XIS 0 plus XIS 3) and XIS-BI spectra jointly with an absorbed blackbody plus power-law, a typical empirical spectral decomposition for magnetars. A multiplicative constant factor was used to account for calibration uncertainties between XIS-FI and XIS-BI, which were $< 3\%$. As presented in Figure 2, we found a good fit ($\chi^2_\nu = 0.96$ with 603 degrees of freedom) with an hydrogen column density of $N_{\text{H}} = (0.89 \pm 0.08) \times 10^{22} \text{ cm}^{-2}$, a photon-index of $\Gamma = 2.8 \pm 0.1$, and a blackbody temperature and radius of $kT = 0.69 \pm 0.01$ keV and $3.2 \pm 0.2 d_{10} \text{ km}$, respectively, where d_{10} is the source distance in units of 10 kpc. The observed and unabsorbed 0.5–10 keV fluxes were $3.8(1) \times 10^{-11}$ and $8.7(8) \times 10^{-11} \text{ erg s}^{-1} \text{ cm}^{-2}$, respectively. While a good fit was also found using a resonant cyclotron scattering model (Rea et al. 2008), a two-blackbody model was unsuccessful. The HXD results on the persistent emission will be reported elsewhere.

3.2. The powerful burst and its light curves

Among the 32 bursts detected by the XIS (§ 3.1), four were also detected by HXD-PIN, and three of them by HXD-GSO, all with $> 3\sigma$ significance. As shown in Figure 3 with a red arrow, the largest event on 2008 August 26 at 03:16:16.947 (UTC) was detected by all the *Suzaku* instruments, including the four HXD-WAM. It was also

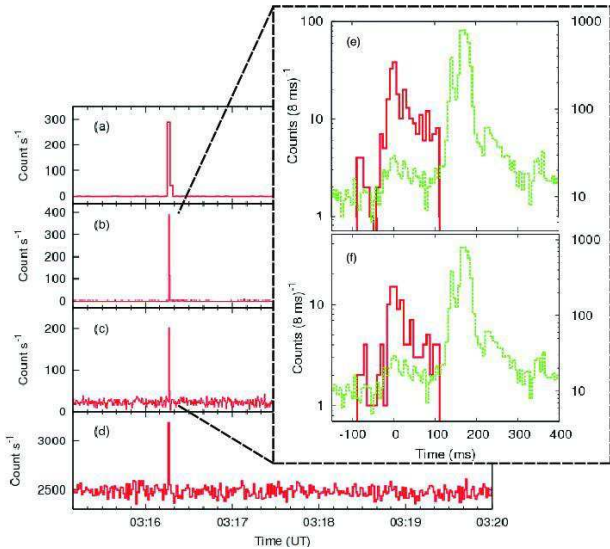


FIG. 3.— Background-inclusive and dead-time-uncorrected light curves of the largest burst. (a) The summed 0.6–10 keV XIS data per 2 s (§ 3.3). (b), (c) HXD-PIN (10–50 keV) and HXD-GSO (50–250 keV) data, respectively, with 0.5 s binning. (d) The 28–111 keV HXD-WAM data with 1 s binning. Panels (e) and (f) are expanded views of (b) and (c), respectively, using 8 ms binning (left ordinate), where the 18–1160 keV *Konus-Wind* light curve (V. Palshin, private communication 2008) is superposed in green (right ordinate).

observed by the *Konus-Wind* instrument (Palmer 2008). The HXD-PIN and HXD-GSO light curves are rather similar with negligible relative delays (within ± 8 ms), indicating that the spectrum is not significantly time-dependent.

The HXD-PIN signal intensity at the peak and that averaged over the ~ 200 ms duration are ~ 38 and ~ 10 counts per 8 ms, which translate to a source intensity of ~ 89 and ~ 23 Crab, respectively. Up to time $t \sim 107$ ms, these light curves are relatively free from instrumental dead times ($\lesssim 6\%$), which have three components (Takahashi et al. 2007); processing times in the analog electronics (HXD-AE), the limited transfer rate from HXD-AE to the digital electronics (HXD-DE), and that from HXD-DE to the spacecraft data processor.

At $t \sim 107$ ms, the HXD signals suddenly terminated. This is an instrumental effect, caused by the second and third factors above, including a forced “flush” of an HXD-DE output buffer. The number of “lost” HXD events can be estimated from various scalar information. Over a 4-s interval including the burst, we found that HXD-PIN received $\sim 14,000$ photons, of which only ~ 250 , or $\sim 2\%$, were duly processed onboard and edited into the light curve. This fraction is similar in the HXD-GSO data, 2.7% (195 processed vs. 7164 received).

By comparing these *Suzaku* light curves with the *Konus-Wind* data (green in Fig. 3e and 3f), we found that the time history observed by the HXD is a “precursor” event. When the much stronger main burst began at $t \sim 138$ ms, the HXD data became completely suppressed, until they returned to normal at $t = 740$ ms. This is consistent with the main burst duration, $\lesssim 0.5$ s, recorded by *Konus-Wind*. The entire burst thus contained ~ 50 times more photons in the hard X-ray band than actually detected by the HXD.

In the XIS data, this burst was split into two readout

frames of 2 s each. We accumulate the XIS data over the 4 s, which contains not only the precursor but also the large main peak (missed by the HXD). Around the XIS image centroid, the very high burst intensity caused strong event pile-up, and telemetry saturation which in turn caused some truncation of the XIS frame readout.

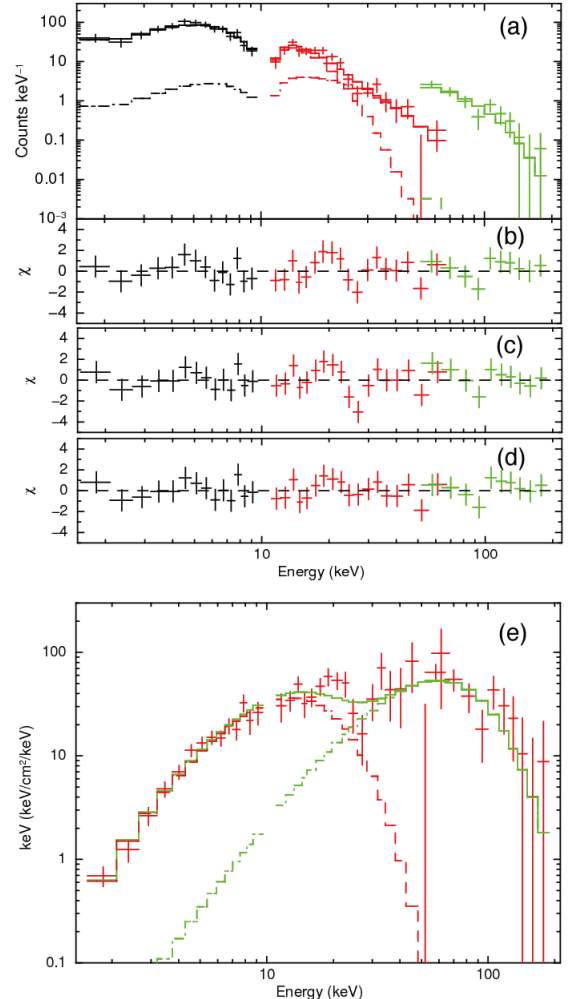


FIG. 4.— (a) Background-subtracted broad-band spectra of the largest burst, fitted by a two blackbody model. Black, red, and green specify XIS-FI, HXD-PIN, and HXD-GSO, respectively. The ordinate is not divided by exposure. (b) Residuals from the fit in panel a. (c)(d) The same as panel b, but when using *CompTT* and *CompTT* \times *cyclabs* models, respectively. (e) The νF_ν plot corresponding to panel a. The XIS data points are scaled to 6% of those in panel (a).

3.3. The burst spectra

Figure 4a shows the spectra of the largest burst, where the ordinate is counts per unit energy (not divided by exposure). The HXD data were accumulated over a time interval of ~ 200 ms around the burst arrival time (see Figure 3). We subtracted the HXD-GSO background (22 count s^{-1} , 50–250 keV) using a 400 s interval before and after the burst. The HXD-PIN background ($0.56 \text{ count s}^{-1}$, 10–70 keV) was negligible. Thus, the emission is detectable up to ~ 200 keV.

The XIS spectra in Figure 4a were accumulated from XIS-FI over the two frames containing the burst. Unlike the HXD data which cover only the precursor, the

XIS events must be dominated by the main burst. To avoid the pile-up and readout truncation problems, we extracted the XIS 0 events using an annulus between radii of $2'$ and $4'.5$, and XIS 3 events between $3'$ and $4'.5$. The two XIS-FI cameras thus yielded 515 burst photons, among which pile-up events are estimated as $<20\%$. We generated particular XIS ancillary response files that correctly reproduce the fraction of photons falling onto these limited accumulation regions.

To evaluate the precursor spectrum, we jointly fitted the HXD-PIN (10–70 keV) and the HXD-GSO (50–250 keV) spectra. The 1–10 keV XIS-FI data were also incorporated, assuming that the precursor has nearly the same spectrum as the much brighter main burst. To take into account the various uncertainties in the HXD and XIS data processing, we left relative model normalizations free between them. The interstellar absorption was fixed at $0.89 \times 10^{22} \text{ cm}^{-2}$ as specified by the persistent emission.

As shown in Figure 4, a model comprising two blackbodies (typical for magnetars bursts; e.g. Olive et al. 2004; Feroci et al. 2004; Nakagawa et al. 2007; Israel et al. 2008b; Esposito et al. 2008) reproduced the data fairly well with $\chi_\nu = 41.0/35 = 1.17$. The deconvolved νF_ν spectra are shown in Figure 4e. The fit yielded two temperatures: $3.3_{-0.4}^{+0.5} \text{ keV}$ and $15.1_{-1.9}^{+2.5} \text{ keV}$. Assuming spherical emission regions, the the cooler and hotter blackbodies are estimated to have radii of $8.0_{-2.1}^{+2.9} d_{10} \text{ km}$ and $0.46_{-0.14}^{+0.16} d_{10} \text{ km}$, respectively. The average (over the 200 ms) and peak 1–200 keV fluxes of the precursor are 1.0×10^{-6} and $3.8 \times 10^{-6} \text{ erg s}^{-1} \text{ cm}^{-2}$, respectively, and the corresponding fluence is $2.0 \times 10^{-7} \text{ erg cm}^{-2}$. The total burst fluence is estimated to be ~ 50 times higher. The model normalization for the HXD data (PIN and GSO together) was $\sim 6\%$ of that of XIS-FI.

When a thermal Comptonization model, `CompTT`, is alternatively used, the fit becomes slightly worse ($\chi_\nu = 42.8/35 = 1.22$; Fig. 4c).

Although the above models are roughly successful for the burst spectrum, a hint of negative residuals is present at $\sim 26 \text{ keV}$ (Fig. 4b), where the two blackbodies cross over. Applying a Gaussian absorption (`Gabs`) or cyclotron absorption (`Cyclabs`) factor at $\sim 26 \text{ keV}$, the fit was improved to $\chi_\nu = 0.89$ (Fig. 4d). However, its addition is significant only at 1.9σ level.

4. DISCUSSION

SGR 0501+4516 was observed by *Suzaku* four days after the burst activation at a flux level of $\sim 3.8 \times$

$10^{-11} \text{ erg s}^{-1} \text{ cm}^{-2}$ (0.5–10 keV). The persistent 0.5–10 keV spectrum obtained with the XIS is described by a $kT = 0.69 \text{ keV}$ blackbody plus a $\Gamma \sim 2.8$ power-law.

If the identification of SGR 0501+4516 with the *ROSAT* source 2RXP J050107.7+451637 (Kennea & Mangano 2008) is correct, the unabsorbed 0.2–10 keV flux increased by a factor ~ 15 with respect to the 1992 value (for a power-law model). Large spectral and flux variations have been recorded in other SGRs as well, in coincidence with the onset of phases of bursting activity. The two most active repeaters, SGR 1806–20 and, to a lesser extent, SGR 1900+14, are known to undergo rather gradual variations in luminosity and spectral properties. In fact, prior to the Giant Flare of 2004 December 27th (Hurley et al. 2005; Palmer et al. 2005), SGR 1806–20 exhibited a factor ~ 2 flux increase and a decrease in Γ from ~ 2 to ~ 1.6 (Mereghetti et al. 2005). In the case of SGR 1900+14 in 2006, the spectral index went from ~ 2.4 to ~ 2 and the flux increased by $\sim 40\%$ (Israel et al. 2008b). In contrast, sources which experience long stretches of quiescence show much more dramatic changes. In May 2008, when SGR 1627–41 reactivated after more than 10 yrs, its Γ switched from ~ 3.3 to ~ 1.5 , and the observed 2–10 keV flux increased by a factor of 40 (Esposito et al. 2008). While the luminosity increase in SGR 0501+4516 is not dissimilar to that of SGR 1627–41, while in outburst its persistent spectrum is much softer.

Among other short X-ray bursts from SGR 0501+4516, we detected a very powerful one, observed also by *Konus-Wind* (V. Palshin private communication 2008). The 1–200 keV precursor spectrum detected with the XIS and the HXD was fitted reasonably well by the two blackbody model. One possible interpretation of the two temperatures ($\sim 3 \text{ keV}$ and $\sim 15 \text{ keV}$) is that they represent the photospheres of the ordinary and extraordinary modes (Harding & Lai 2006; Israel et al. 2008b), which can have different radii and temperatures due to suppression of extraordinary-mode scattering and photon-splitting in the super-critical magnetic field.

We thank Dr. Valentin Pal'shin and Dr. Dmitry Frederiks for allowing us to use their *Konus-Wind* light curve prior to publication. Our thanks are also due to the *Suzaku* operation team, who successfully conducted the ToO observation. NR is supported by an NWO Veni Fellowship, DG thanks the CNES for financial support, and SZ acknowledges support from STFC.

REFERENCES

- Barthelmy, S. D., et al. 2008, GCN Circ., 8113, 1
Dall'Osso, S., Israel, G. L., Stella, L., Possenti, A., & Peruzzi, E. 2003, ApJ, 599, 485
Esposito, P., et al. 2008, MNRAS, 390, L34
Feroci, M., Caliendo, G. A., Massaro, E., Mereghetti, S., Woods, P. 2004, ApJ, 612, 408
Göğüş, et al. 2008, The Astronomer's Telegram, 1677
Harding, A. K., & Lai, D. 2006, Reports on Progress in Physics, 69, 2631
Holland, S. T., & Sato, G. 2008, GCNR, 160, 1-2
Hurley, K., et al. 2005, Nature, 434, 1098
Israel, G. L., et al. 2008a, The Astronomer's Telegram, 1692
Israel, G. L., et al. 2008b, ApJ, 685, 1114
Kennea, J. A., & Mangano, V. 2008, The Astronomer's Telegram, 1675
Koyama, K. et al. 2007. PASJ 59, S23
Mereghetti, S. 2008, A&A Rev., 15, 225
Mereghetti, S. et al. 2005, ApJ, 628, 938
Mitsuda, K. et al. 2007. PASJ 59, S1
Nakagawa, Y. E. et al. 2007, PASJ, 59, 653
Olive, J.-F. et al. 2004, ApJ, 616, 1148
Ouyed, R., Leahy, D., & Niebergal, B. 2007, A&A, 473, 35
Palmer, D. 2008, The Astronomer's Telegram, 1683
Palmer, D. M. et al. 2005, Nature, 434, 1104
Rea, N., et al. 2008, ApJ, 686, 1245
Takahashi, T. et al. 2007. PASJ 59, S35
Thompson, C., & Duncan, R.C. 1995, MNRAS, 275, 255
Woods, P.M. & Thompson, C. 2006, Compact stellar X-ray sources. Ed. W. Lewin & M. van der Klis, Cambridge University Press